# Magnetic Resonance Images of Coarsening Inside a Foam

C. P. Gonatas,[1,*]. J. S. Leigh,[2] and A. G. Yodh[1]

[1]*Department of Physics, University of Pennsylvania, Philadelphia, Pennsylvania 19104*
[2]*Department of Radiology, University of Pennsylvania, Philadelphia, Pennsylvania 19104*

James A. Glazier and B. Prause

*Department of Physics, University of Notre Dame, Notre Dame, Indiana 46556*
(Received 13 September 1994; revised manuscript received 2 May 1995)

Coarsening in three-dimensional polycrystalline systems such as foams, magnetic bubbles, metal crystals, and ceramics is poorly understood because of the absence of data describing the interior of these materials. We introduce *magnetic resonance imaging* to probe the interior of a foam, providing information on topology and foam drainage. The foam does not appear to coarsen in a self-similar way during observation periods of up to 50 h, representing over a decade of growth in the mean length scale.

Though we encounter foams every day, their structure and rheological properties are difficult to explain. The viscosity of foam is much greater than the viscosity of its liquid and gas constituents and, unlike a liquid, foams have a nonzero yield stress. These unusual properties make foams useful as drilling fluids in oil recovery, for fire fighting, and for shaving. Although recent simulations explain some properties in terms of the constraints on fluid motion due to structure [1], the structure is rarely well characterized and changes dynamically through coarsening.

Despite its simplicity, the structure of three-dimensional foams is not understood, in part because of the difficulty of visualizing their interior. Plateau borders, the accumulation of fluid between bubbles, scatter light so strongly that optical photographs can only probe the surface layer of bubbles.

Recent experiments with diffusing light probes infer mean bubble sizes and dynamics [2]. However, this technique is somewhat model dependent and does not provide direct information on bubble size distributions or topology. Insertion probe sampling provides additional information but destroys the sample as measurements progress [3]. To circumvent these difficulties, we introduce magnetic resonance imaging (MRI) as a noninvasive probe of the foam interior. MRI provides nondestructive visualization of the foam by sampling the polarization density of the nuclear moment as a function of position. This enables us to reconstruct the topology at successive stages of coarsening.

The MRI technique is well known for its use in hospitals; however, it has recently found applications such as in engineering studies of porous media. In the present experiment we used a 1.8 T medical MRI spectrometer to image protons by selectively exciting a two-dimensional slice and resolving the transverse dimensions by frequency and phase encoding [4]. A foam is a particularly difficult object to image because MRI can only detect the liquid content, and a dry foam may contain only 5% liquid. In addition, foams have structure on the order of a few hundred microns or less, well below the 1 mm resolution of most medical MRI. Despite our use of a low field instrument, we achieved 100 $\mu$m resolution by optimizing the rf antenna that detects the NMR signals and by optimizing the pulse sequences that encode spatial information into the NMR signal. The spatial scale was calibrated using water-filled capillary tubes at a 2 mm separation. Each image was acquired during a spin echo pulse sequence consisting of 128 individual phase encode sequences, with a spin echo time of 10 ms.

The studies used a whipped gelatin foam (Norland Products HiPure, New Brunswick, NJ; 45% concentration). This gelatin is formulated for long life and stability, and does not separate or polymerize even after many months at room temperature. A strongly paramagnetic salt, $DyCl_3$, was added in a 15 m$M$ concentration to null the magnetic susceptibility of the liquid, eliminating effects due to the liquid/air mismatch. We added an equal molar amount of triethylenetetramine-hexacetic acid (TTHA) (Sigma Chemical) to chelate the rare earth salt, aiding its solubility. Because of the susceptibility matching, the primary magnetic field through the sample was so uniform that the NMR linewidth was only 40 Hz, negligibly small compared to the 100 Hz width of each pixel in the frequency encode axis. Finally, we added a small quantity of $CuSO_4$ to increase the longitudinal NMR spin relaxation rate, enabling us to increase the repetition rate of the NMR pulse sequence.

The solution was whipped into a cream, allowed to evolve for several hours, and then inserted into a 1.4 cm diameter sample cell. Samples prepared in this way could last up to a week. Initial bubble sizes ranged from 0.01 to 0.2 mm, as determined by inspection with a light microscope. Average bubble diameters for the initial state were 0.07 mm. During the first few hours, the foam coarsened rapidly to a point where we could measure the bubbles easily with MRI. For the run we describe in greatest detail, we began observations 12 h after initial sample preparation. The foam drained

continuously during observations. We monitored the drainage periodically, using one-dimensional scans of the liquid density in the vertical direction.

In Fig. 1 we show two maps at different times of the same horizontal foam slice. The sensitivity of the instrument is sufficient to resolve some of the films between the bubbles. Figure 1(a) was taken at the beginning of our observations, 760 min after initial sample preparation; Fig. 1(b) was observed 3250 min after Fig. 1(a). Figure 1(b) shows very large bubbles, which are absent in Fig. 1(a). However, small bubbles persist at all times. In all foams, coarsening results simply from gas diffusion between bubbles due to small pressure differences caused by bubble curvature. One-dimensional NMR profiles have been used to probe foam structure [5], but to our knowledge, these are the first images of coarsening inside a foam.

The composition of the foam affects the growth rate in two related ways. The viscosity and gas solubility of the liquid determine the gas diffusion constant. Pressure differences between bubbles are determined by relative wall curvatures and the surface tension of the liquid. The surface tension is intrinsic to the liquid, and together with the other intrinsic factors, determines the rate of coarsening. The sequence of topological distributions and correlations does not depend on the rate of coarsening. Experimentation in various 2D froths with different fixed coarsening rates has shown that coarsening rate does not affect the self-similar nature of growth or the values of growth exponents [6].

The change in liquid fraction due to drainage accelerates growth because gas diffuses more rapidly between thinner bubble membranes and plateau borders, so we consistently overestimate the natural growth rate of the foam. However, as outlined above, change in growth rate does not affect topology [7]. Thus our fits for growth exponents suggest an upper bound to the natural growth exponent (i.e., the exponent in the absence of drainage). An accelerating time scale for coarsening does not affect self-similarity of growth, if growth is self-similar in the absence of drainage.

We analyze each image by fitting circles to each bubble to determine its location and size. When the films between cells are not visible, we infer the presence of a bubble from its plateau borders. The method is approximate. Because of the finite voxel resolution, described in Table I, we could only realistically fit bubbles greater than 250 $\mu$m in diameter. Also, polygonal bubbles are not always well fitted by a circle. Where single circles give poor fits, we permit small overlaps in adjacent fitted
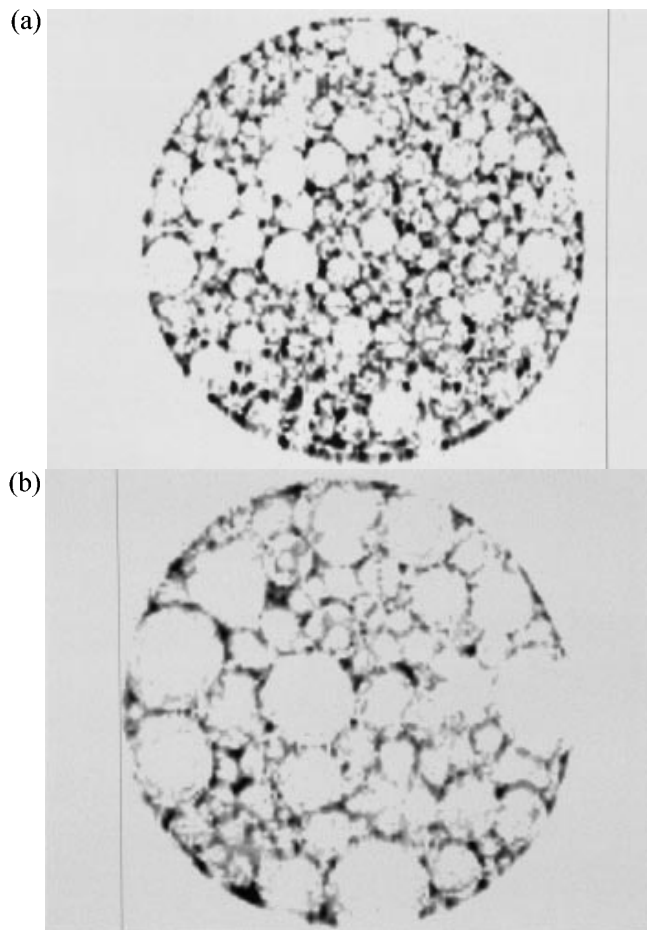


FIG. 1. (a) Horizontal foam cross section, 3 mm from bottom of cell at 263 min from beginning of observations. (b) Same cross section, 3250 min from beginning of observations. Scale is given by 1.4 cm inner diameter of sample cell.

bubbles so that the area of the fitted circle equals the area of the bubble. The resulting histograms of the size distributions give a detailed description of the foam interior. In Fig. 2 we show examples of the bubble size distribution at 25 and 3250 min. Though both histograms show a majority of bubbles at small sizes, the late histogram shows an extended tail of bubbles that cover most of the surface area. The growth does not appear to be self-similar. That is, we cannot simply rescale the bubble radius by a multiplicative factor to obtain the late-time distribution from the early distribution. In the inset to Fig. 2 we show the drainage, which reduces the liquid fraction from 10% to 5%, suggesting the foam is in the "dry" limit [8] as opposed to the "wet" limit described by Lifshitz-Slyozof growth [9].

TABLE I. Instrumental resolution.

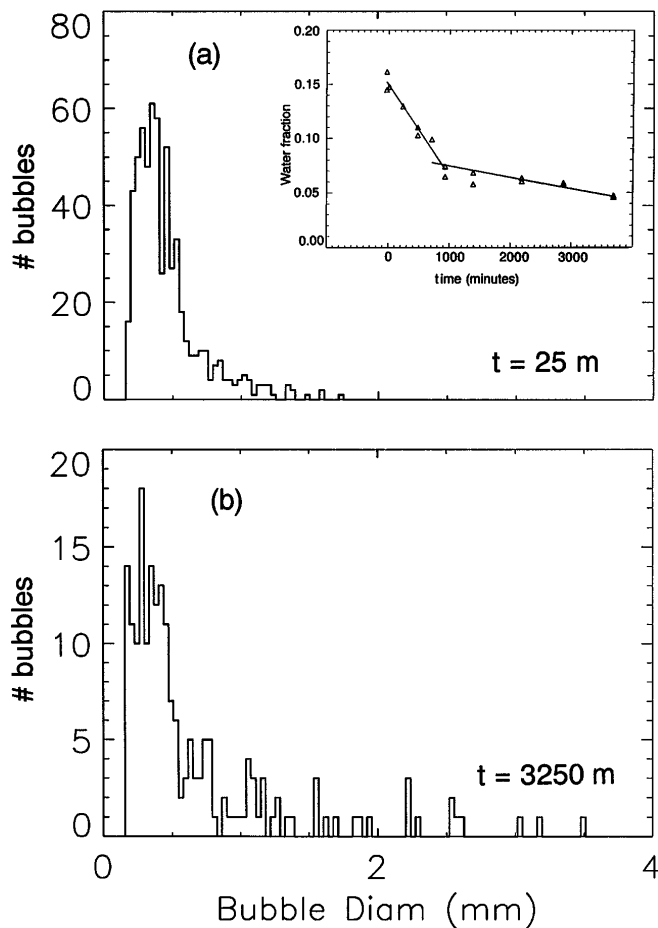| Time (min) | Slice thickness (cm) | Frequency encode resolution (cm) | Phase encode resolution (cm) |
|---|---|---|---|
| 0–745 min | 0.011 | 0.010 | 0.013 |
| 746–3300 min | 0.019 | 0.010 | 0.013 |

FIG. 2. Bubble size distribution at succesive times of same cross section as Fig. 1 (a) at $t = 25$ min, (b) at $t = 3250$ min. Note the extended tail of large bubbles in (b). Inset: liquid fraction in foam slice vs time. Linear fits to drainage rates are superposed.

In these initial experiments we reduced the amount of data by averaging between 20 and 50 individual images at a time and by tracing the evolution only of single image slices. Thus, we miss effects due to rapid rearrangements, and we introduce a systematic shift in the distribution because of the sectioning. Given a bubble of radius $r$, the apparent radius $r_{proj}$ depends on where the section intersects the bubble. Sectioning results in a distribution of $r_{proj}$ up to a maximum of $r$, with $\langle r_{proj} \rangle = \pi r/4$. Modeling showed that projection increases the higher moments of the distribution by a multiplicative constant nearly independent of the distribution. Most importantly, in self-similar growth where $\rho_{true}(r, t) = \rho_{true}(\gamma \times r, t')$, with $\gamma$ a constant, $\gamma$ also scales the observed distribution as $\rho_{proj}(r, t) = \rho_{proj}(\gamma \times r, t')$. Thus, without deconvolution we can estimate scaling exponents and higher moments, and determine whether or not growth is self-similar.

A simplifying assumption for 3D froth, which holds for 2D froth at long enough times [10], is that the mean radius obeys power law growth given by $\langle r \rangle \sim$

$(t - t_0)^{\beta}$. Although our dynamic range of growth is limited, we estimate $\beta = 0.3 \pm 0.1$, consistent among several independent runs. A scaling argument predicts the growth exponent for the mean bubble area, $\alpha = 2\beta = 1$, so we can compare the growth of $\langle A \rangle$ to a line with positive slope, regardless of assumptions for $t_0$. We show the growth in mean bubble area, $\langle A \rangle$, in Fig. 3.

The most significant characteristic of the bubble size distribution is its dimensionless second moment

$$\mu_2 \equiv \frac{\sqrt{\langle r^2 \rangle - \langle r \rangle^2}}{\langle r \rangle}, \quad (1)$$

where $\langle \rangle$ denotes an average over the bubble size distribution. For self-similar growth, $\mu_2$ is constant. In Fig. 4 we show the evolution of $\mu_2$. Even after 1000 min of observation, $\mu_2$ continued to increase. We conclude that our sample did not attain self-similar growth within 50 h, representing over a decade of growth from the initial preparation.

In Fig. 3 we illustrate the effect of systematic errors by measuring the bubble sizes two different ways. In the first, the fitting permitted significant overlaps of bubbles (asterisks). In the second, the fitting excluded overlaps except for large, obviously polygonal bubbles (triangles). The mean sizes calculated, allowing overlaps, are systematically larger, but the relative growth is the same.

The finite resolution of our current measurement introduces a potential source of systematic error. If we miss substantial numbers of very small bubbles, our estimates of mean bubble sizes and higher moments could be skewed. Microscope photographs of newly prepared foams indicate that all bubbles are initially smaller than 200 $\mu$m, only twice the size of our minimum resolution pixel. The foam coarsens rapidly during an initial period, so that 4 h after sample preparation, sequences of microscope photographs reveal that only 25% of the bubbles are smaller than 200 $\mu$m. This fraction declines to 15% at 12 h, corresponding to the initial time of NMR observations, and declines imperceptibly for the next 12 h. To model the effect of the missing bubbles, as a severe case
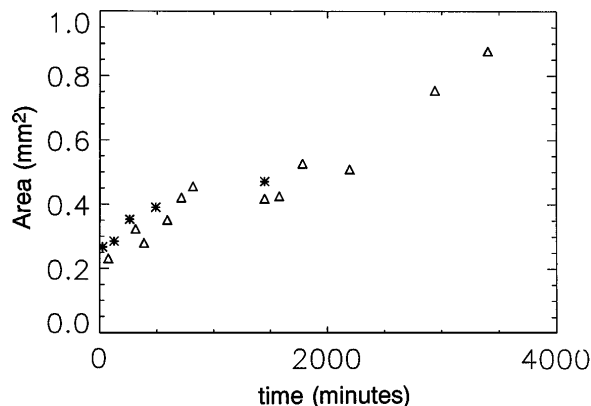


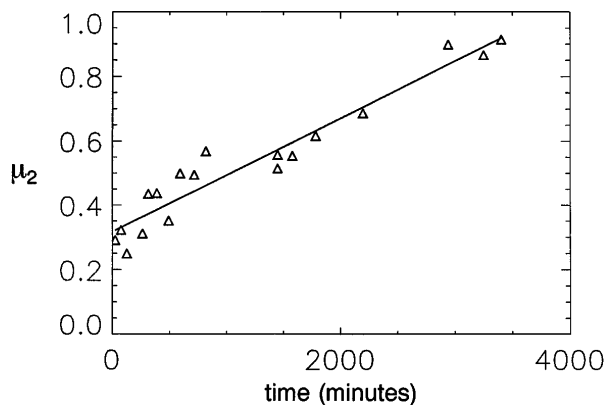FIG. 3. Growth of average bubble area $\langle A \rangle$ vs time.

FIG. 4.  Plot of second moment of distribution, $\mu_2$, vs time. Linear fit is superposed.

we added 15% more bubbles to the size distributions, all at 50 $\mu$m diameter. The first moments decrease systematically by about 15% for all times. The second moment $\mu_2$ increases by 10% to 20%, depending on the evolution time. The tendency of the missing bubbles to increase $\mu_2$ at late times relative to the early times is small (about 15%), compared to the large increase in $\mu_2$ we observed throughout several different NMR runs. We conclude that the missing bubbles do not affect the moments very much, so that undercounting does not materially change the most important observation of this paper. It has been suggested that all dry foams attain self-similar growth [10]. This expectation derives in part from the observation of a scaling state at long times in 2D foams [6]. However, 3D simulations suggest that the three-dimensional foam takes much longer than a two-dimensional foam to reach a scaling state, equilibrating only after the characteristic length increases by two orders of magnitude [11,12]. Light scattering measurements of 3D foam [2] suggest that a scaling state is reached with exponent $\alpha = 1/2$ after an increase of only 10% in length scale occurring within 10 min (for Gillette Foamy Regular). While we do not exclude the possibility of self-similar growth at long times, our measurements are more consistent with the recent simulations than with the recent inference of a scaling state in Gillette Foamy Regular. The foam length scale in our experiment increases by about an order of magnitude from initial preparation *without* reaching a state of self-similar growth.

*Current address: Exxon Research and Engineering Co., Annandale, NJ 08801.

[1] D. A. Reinelt and A. M. Kraynik, J. Colloid Interface Sci. **159**, 460 (1993); A. M. Kraynik, Annu. Rev. Fluid Mech. **20**, 325 (1988).

[2] D. J. Durian, D. A. Weitz, and D. J. Pine, Science **252**, 686 (1991); J. Phys. Condens. Matter **2**, SA433 (1990).

[3] C. G. J. Bisperink, J. C. Akkerman, A. Prins, and A. D. Ronteltap, Food Struct. **11**, 101 (1992).

[4] P. T. Callaghan, *Principles of Nuclear Magnetic Resonance Microscopy* (Clarendon Press, Oxford, 1991).

[5] M. McCarthy, J. Am. Inst. Chem. Eng. **36**, 287 (1990).

[6] J. A. Glazier, S. P. Gross, and J. Stavans, Phys. Rev. A **36**, 306 (1987).

[7] For sufficiently wet froth, P. Bolton and B. Weaire [Philos. Mag. B **63**, 795 (1991)] have pointed out that the finite size of Plateau borders affects growth rates of individual bubbles by perturbing the curvature of cell walls. The largest concentrations of liquid distort wall curvature the most, however, these are distributed randomly. Therefore, *average* growth rates for bubbles of a given size are not affected.

[8] J. Stavans and J. A. Glazier, Phys. Rev. Lett. **62**, 1318 (1989).

[9] IK. M. Lifshitz and V. V. Slyozof, JETP Lett. **35**, 331 (1959).

[10] J. A. Glazier and D. Weaire, J. Phys. Condens. Matter **4**, 1867 (1992); J. Stavans, Rep. Prog. Phys. **56**, 733 (1993).

[11] M. P. Anderson, G. S. Grest, and D. J. Srolovitz, Philos. Mag. **59**, 293 (1989).

[12] J. A. Glazier, Phys. Rev. Lett. **70**, 2170 (1993).